D 7 Quasielastic Scattering [1]

Joachim Wuttke
Jülich Centre for Neutron Science at FRM II
Forschungszentrum Jülich GmbH

Contents

[1] Lecture Notes of the 43rd IFF Spring School "Scattering Methods for Condensed Matter Research: Towards Novel Applications at Future Sources" (Forschungszentrum Jülich, 2012).

1 Introduction

The term 'quasielastic scattering' designates a limiting case of inelastic scattering that is close to elastic scattering. There are different ways to specify what 'close' means. In a wider sense, it is only required that the energy transfer be small compared to the incident energy of the scattered particles. This is how the word 'quasielastic' originally was coined in nuclear physics. In a narrower sense, a *quasielastic line* is a spectral feature centered around the elastic peak. A very special use or abuse of the term 'quasielastic' shall only be mentioned in passing: *quasielastic light scattering*, also called *dynamic light scattering* or (much more to the point) *photon correlation spectroscopy*.[2]

Quasielastic neutron scattering (QENS) is used to study atomic and molecular modes of motion that are slower than the phonons typically studied on a triple-axis spectrometer. A lower bound for the energy transfers is set by the resolution of available spectrometers. In the following, we will only discuss energy-resolved measurements on time-of-flight or backscattering spectrometers, refering to another lecture (D8) for the spin-echo method, which is special in several respects (implicit Fourier transform, preference for coherent scattering, focus on small q). Accordingly, we are concerned with energy transfers of the order of μeV to meV, corresponding to time scales of ns to ps. Motion on this time-scale involves molecular reorientations and certain slow oscillations as well as jump processes that add up to diffusion or relaxation.

Depending on the isotopic composition of the sample, neutron scattering can be dominated by coherent or incoherent contributions (lecture A4). Coherent scattering conveys richer information, but is more difficult to interpret. On time-of-flight and backscattering spectrometers, by far the majority of experiments is concerned with incoherent scattering. In particular, whenever a sample contains hydrogen, this element is likely to dominate the total cross section, except if the material is fully deuterated. In this lecture we will concentrate on the most simple and most important use of QENS: *incoherent scattering* by *hydrogen*.

2 Basics

2.1 Self correlation functions

Incoherent neutron scattering measures *self correlations* of *tagged particles*. Assuming that there is just one noteworthy species of scatterers, the double differential cross section can be written as[3]

$$\frac{\partial^2\sigma}{\partial\Omega\partial\omega} = \frac{\sigma_{\mathrm{inc}}}{4\pi}\frac{k_{\mathrm{f}}}{k_{\mathrm{i}}}S_{\mathrm{inc}}(\mathbf{Q},\omega). \tag{1}$$

For the remainder of this lecture, the subscript 'inc' will be omitted. Let us summarize a few relations from lecture A5. The *scattering function* $S(\mathbf{Q},\omega)$ is best expressed via a Fourier transform in time,

$$S(\mathbf{Q},\omega) = \frac{1}{2\pi}\int \mathrm{d}t\, \mathrm{e}^{-i\omega t}\, I(\mathbf{Q},t), \tag{2}$$

[2] In photon-correlation spectroscopy, scattered photons are counted regardless of their energy; photon counts are then correlated by some real-time electronics. This has almost nothing in common with quasielastic neutron scattering. The light scattering analogue of quasielastic neutron scattering is called high-resolution inelastic light scattering or *Rayleigh-Brillouin scattering*; to analyse the energy of scattered photons either a Fabry-Perot interferometer or a high-resolution grating spectrometer is used.

[3] Only here, Ω stands for a solid angle. Later on, we will reuse the symbol Ω to designate characteristic frequencies of our model systems.

with the *intermediate scattering function*

$$I(\mathbf{Q},t) = \frac{1}{N}\sum_j \left\langle \mathrm{e}^{-i\mathbf{Q}\hat{\mathbf{r}}_j(0)}\mathrm{e}^{i\mathbf{Q}\hat{\mathbf{r}}_j(t)}\right\rangle . \tag{3}$$

Its initial value is $I(\mathbf{Q},0) = 1$. In the ballistic short-time regime (for times that are short compared to a typical phonon period), it has the expansion

$$I(\mathbf{Q},t) = \frac{1}{N}\sum_j \left\langle \mathrm{e}^{i\mathbf{Q}\mathbf{v}_j(0)}\right\rangle \doteq 1 - \frac{1}{2}\Omega_Q^2 t^2 + \ldots \tag{4}$$

with a frequency Ω_Q that depends on Q and on the mean squared thermal velocity:

$$\Omega_Q^2 := \frac{1}{N}\sum_j \left\langle (\mathbf{Q}\mathbf{v}_j(0))^2\right\rangle = \frac{Q^2}{3}\frac{1}{N}\sum_j \left\langle \mathbf{v}_j(0)^2\right\rangle = Q^2 k_\mathrm{B}T\frac{1}{N}\sum_j \frac{1}{m_j}. \tag{5}$$

Since Ω_Q lies far outside the dynamic range of the spectrometers used for QENS, the short-time expansion has only theoretical importance.

An additional Fourier transform in space,

$$I(\mathbf{Q},t) = \int \mathrm{d}^3 r\, \mathrm{e}^{i\mathbf{Q}\mathbf{r}}\, G_\mathrm{s}(\mathbf{r},t) \tag{6}$$

relates the intermediate scattering function to the self-correlation function

$$G_\mathrm{s}(\mathbf{r},t) = \frac{1}{N}\sum_j \int \mathrm{d}^3 r'\ \left\langle\, \delta(\mathbf{r}-\mathbf{r}'+\hat{\mathbf{r}}_j(0))\, \delta(\mathbf{r}'-\hat{\mathbf{r}}_j(t))\,\right\rangle . \tag{7}$$

Before taking the classical limit, it is advisable to correct for detailed balance, introducing the symmetrized scattering law

$$\tilde{S}(\mathbf{Q},\omega) := \mathrm{e}^{\hbar\omega/2k_\mathrm{B}T} S(\mathbf{Q},\omega). \tag{8}$$

In the classical limit, the position operators commute, and the symmetrized self-correlation function $\tilde{G}_\mathrm{s}$ is approximated by

$$G_\mathrm{s}^\mathrm{cl}(\mathbf{r},t) = \frac{1}{N}\sum_j \left\langle\, \delta(\mathbf{r}-\hat{\mathbf{r}}_j(t)+\hat{\mathbf{r}}_j(0))\,\right\rangle . \tag{9}$$

2.2 Harmonic vibrations and the mean squared displacement

Before turning to the slow, anharmonic modes of motion that are typically studied by QENS, we briefly review scattering by harmonic vibrations (compare lecture B4). This analytically tractable reference case helps us to introduce important concepts like elastic incoherent structure factor and the mean squared displacement, which later on will be generalized for non-harmonic systems.

Vibrations are described in terms of displacements $\mathbf{u}_j(t)$ from equilibrium positions $\mathbf{R}_j$,

$$\mathbf{r}_j(t) = \mathbf{R}_j + \mathbf{u}_j(t). \tag{10}$$

Eq. (3) keeps its form under this transformation, except that the $\mathbf{r}_j$ are substituted by $\mathbf{u}_j$. If the particles j are only subject to harmonic forces, then the Bloch theorem [1] allows the simplification

$$I(\mathbf{Q},t) = \frac{1}{N}\sum_j \mathrm{e}^{-2W_j(\mathbf{Q},\mathbf{0})}\mathrm{e}^{2W_j(\mathbf{Q},t)} \tag{11}$$

with

$$2W_j(\mathbf{Q},t) := \langle\,(\mathbf{Q}\mathbf{u}_j(0))(\mathbf{Q}\mathbf{u}_j(t))\,\rangle\,. \tag{12}$$

In isotropic systems, an orientational average gives

$$2W_j(Q,t) = \frac{Q^2}{3}\,\langle\,\mathbf{u}_j(0)\mathbf{u}_j(t)\,\rangle\,. \tag{13}$$

Each particle partakes in a huge number of oscillatory modes, which quickly run out of phase. Therefore, within little more than one typical phonon period, $2W_j(\mathbf{Q},t)$ approaches 0. In consequence, the intermediate scattering function converges towards the long-time limit

$$I(\mathbf{Q},t\to\infty) = \frac{1}{N}\sum_j \mathrm{e}^{-2W_j(\mathbf{Q},\mathbf{0})} =: f_{\mathbf{Q}}. \tag{14}$$

This value is called the *Debye-Waller factor*, or, if one wants to emphasize the distinction between incoherent and coherent scattering, the *Lamb-Mössbauer factor* or the *elastic incoherent structure factor* (EISF). The Fourier transform of (11) gives

$$S(\mathbf{Q},\omega) = f_{\mathbf{Q}}\delta(\omega) + (1-f_{\mathbf{Q}})S_{\mathrm{inelast}}(\mathbf{Q},\omega). \tag{15}$$

Here the EISF reappears as the amplitude of the elastic delta line, and its complement as the intensity of the inelastic phonon spectrum. In a first approximation, this spectrum is proportional to the *vibrational density of states* (VDOS) $g(\omega)$, divided by ω^2. As soon as one goes beyond the first approximation, the extraction of a VDOS from inelastic neutron scattering data becomes a tour de force of non-linear, interdependent corrections.

But even the elastic intensity contains *some* information about the VDOS: Assuming that there is just one type of scatterers, Eqs. (13) and (14) provide a simple expression for the *mean squared displacement* (MSD)

$$\langle u_x^2\rangle = \frac{\langle\mathbf{u}^2\rangle}{3} = \frac{-\ln f_Q}{Q^2}. \tag{16}$$

On backscattering instruments, one can rather comfortably measure f_Q as function of temperature T (elastic temperature scan with no Doppler modulation of the incident neutron energy). From the slope of $-\ln f_Q(T)$ versus Q^2 one obtains the MSD.

The MSD in turn is a temperature weighed moment of the VDOS,

$$\langle u_x^2\rangle = \frac{\hbar}{6m}\int \mathrm{d}\omega\,\frac{g(\omega)}{\omega}\coth\frac{\hbar\omega}{2k_\mathrm{B}T}. \tag{17}$$

Approximating the VDOS by the *Debye model*,

$$g_\mathrm{D}(\omega) = \begin{cases} \dfrac{9\omega^2}{\omega_\mathrm{D}^3} & \text{for } 0\le\omega\le\omega_\mathrm{D}, \\ 0 & \text{else,} \end{cases} \tag{18}$$

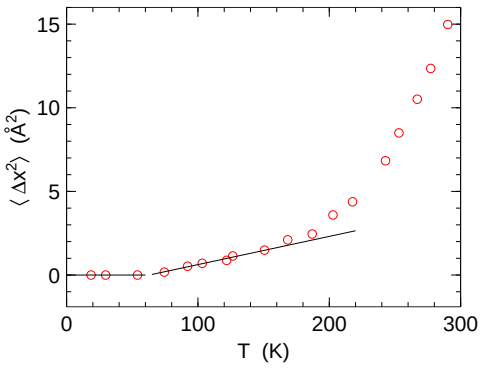

Fig. 1: *Temperature dependence of the mean squared displacement in hydrated myoglobin, measured by thermal neutron backscattering (IN13 at ILL), redrawn from the seminal work by Doster, Cusack, and Petry (1989) [2]. The solid lines indicate the asymptotes (19) expected for harmonic vibrations, with a clear crossover from quantum zero-point oscillations to a linear regime. Anharmonic contribution appear above 150 K, and increase strongly above 180 K. In the last 20 years, this "protein dynamic transition" has been intensely studied, but its nature is still disputed [3].*

and expressing the cut-off frequency $\omega_{\rm D}$ through the equivalent *Debye temperature* $\Theta_{\rm D} := \hbar\omega_{\rm D}/k_{\rm B}$, we find the asymptotes

$$\left\langle u_x^2 \right\rangle \doteq \begin{cases} \dfrac{3\hbar^2}{4mk_{\rm B}\Theta_{\rm D}} & \text{for } T \ll \Theta_{\rm D}, \\ \dfrac{3\hbar^2}{mk_{\rm B}\Theta_{\rm D}}\dfrac{T}{\Theta_{\rm D}} & \text{for } T \gg \Theta_{\rm D}. \end{cases} \tag{19}$$

At $T \simeq \Theta_{\rm D}/4$, the MSD crosses over from temperature-independent quantum zero-point oscillations to a linear temperature dependence. This crossover is indeed regularly observed in the low-temperature part of elastic scans. At higher temperatures, deviations from the linear behavior $\langle u_x^2\rangle \propto T$ reveal the onset of anharmonic motion (Fig. 1).

2.3 Quasielastic broadening; localized versus diffusive motion

The quantum theory of harmonic vibrations has provided us with a clear decomposition (15) of the scattering function into an elastic peak and a broad phonon spectrum. This is no longer the full story if there are non-vibrational degrees of freedom, due for instance to molecular rotation or atomic diffusion. In such cases, the elastic delta function is expected to *broaden* into a quasielastic spectrum. However, if the non-vibrational motion is much slower than typical vibrations, the overall structure of Eq. (15) remains a good approximation:

$$S(\mathbf{Q},\omega) \simeq f_{\mathbf{Q}} S_{\rm QENS}(\mathbf{Q},\omega) + (1-f_{\mathbf{Q}}) S_{\rm inelast}(\mathbf{Q},\omega). \tag{20}$$

If there is no clear separation of time scales, it may be more appropriate to replace $S_{\rm inelast}$ by a convolution $S_{\rm QENS} \otimes S_{\rm inelast}$.

The replacement of $\delta(\omega)$ by $S_{\rm QENS}(\mathbf{Q},\omega)$ does not necessarily mean that there is no more central delta line. In the next section, we will discuss jump and rotator models for which the quasielastic scattering has the form

$$S_{\rm QENS}(\mathbf{Q},\omega) = a_{\mathbf{Q}}\delta(\omega) + b(\mathbf{Q},\omega). \tag{21}$$

The presence of an elastic line ensures that the intermediate scattering function has a nonzero long-time limit $I(\mathbf{Q}, t \to \infty) = f_\mathbf{Q} a_\mathbf{Q}$. This is the defining characteristic of *localized motion*: the scatterers remain confined to a finite region in space. In the opposite case of *long-ranged diffusion*, $I(\mathbf{Q}, t)$ has the long-time limit 0, and S_{QENS} has no delta component.

We also need to generalize the mean squared displacement. It becomes a time-dependent function that can be computed as the second moment of the self-correlation function,

$$\left\langle r^2(t) \right\rangle := \int \mathrm{d}^3 r \, r^2 \, G_\mathrm{s}(\mathbf{r}, t). \tag{22}$$

2.4 Important fit functions

When it comes to fitting QENS data, one usually starts with very simple model functions like a Lorentzian, and in many cases this is all one needs. Let us therefore collect some basic facts about a few fit functions.

Computationally the simplest fit function is the Gaussian. Unfortunately, it has few applications beyond the textbook case of an ideal gas (lecture A5). A normalized Gaussian, as one would use to fit a scattering function, has the standard form

$$\mathcal{G}(\omega; \Gamma) := \frac{1}{\sqrt{2\pi}\Gamma} \mathrm{e}^{-\omega^2/2\Gamma^2}. \tag{23}$$

Its Fourier transform, corresponding to the intermediate scattering function, is also a Gaussian:

$$\tilde{\mathcal{G}}(t; \Gamma) = \mathrm{e}^{-\Gamma^2 t^2/2}, \tag{24}$$

which is perfectly consistent with the short-time expansion (4). The width of a Gaussian spectrum is often expressed by its *full width at half maximum* (FWHM), which can be easily computed as $\sqrt{8 \ln 2}\Gamma$. Intermediate scattering functions are usually characterised by a *mean relaxation time*,

$$\langle \tau \rangle := \int_0^\infty \mathrm{d}t \, I(Q, t) = \pi S(Q, 0). \tag{25}$$

For the Gaussian, one finds $\langle \tau \rangle = \sqrt{\pi/2}/\Gamma$.

Diffusion, jump processes, and rotations can all be modelled by variants of the *master equation*, leading to a *Lorentzian* scattering function. The normalized Lorentzian, in mathematics known as the *Cauchy distribution*, has the form

$$\mathcal{L}(\omega; \Gamma) := \frac{1}{\pi} \frac{\Gamma}{\Gamma^2 + \omega^2}. \tag{26}$$

Its Fourier transform is a simple exponential,

$$\tilde{\mathcal{L}}(t; \Gamma) = \mathrm{e}^{-\Gamma t}. \tag{27}$$

The FWHM is 2Γ, and the mean relaxation time $\langle \tau \rangle = 1/\Gamma$. The exponential (27) is *not* compatible with the short-time expansion of $I(Q, t)$: the master equation does not adequately capture the ballistic short-time regime. The limited range of validity of Lorentzian fits is also obvious from the fact that the Cauchy-Lorentz distribution does not possess a second moment, whereas a sum rule relates the second moment of $S(Q, \omega)$ to the velocity autocorrelation function.

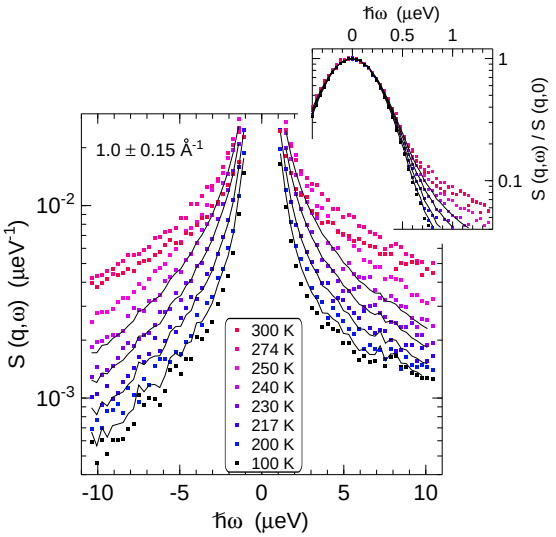

Fig. 2: *Spectra of the hydrated protein c-phycocyanin, measured on the backscattering spectrometer SPHERES of JCNS. Solid lines are fit with a Kohlrausch-Williams-Watts function ($\beta = 0.5$), numerically convolved with the resolution measured at 100 K (black symbols); abover 240 K, this function becomes inadequate, and measurements over a wider energy range are needed to establish a physically valid description of $S(Q,\omega)$. As in many other QENS experiments, quasielastic scattering first appears deep in the wings of the resolution function, whereas no broadening can be seen at half maximum (inset). Redrawn from [4].*

Another important fit function is the *stretched exponential function*, which is defined in the time domain as

$$\tilde{\mathcal{K}}_\beta(t;\tau) := \mathrm{e}^{-(t/\tau)^\beta}. \tag{28}$$

Its Fourier transform, often called the *Kohlrausch-Williams-Watts* function, must be computed numerically except in a few special cases ($\beta = 0.5, 1, 2$). With typical values of β between 0.4 and 0.8, it is often used to describe relaxation in viscous liquids; with the special value $\beta = 0.5$, it includes a key result of the Rouse model for polymer motion. Its characteristic relaxation time is $\langle\tau\rangle = \tau\Gamma(1/\beta)/\beta$ where $\Gamma()$ is the gamma function.

2.5 Instrumental resolution

Every spectrometer has a finite *resolution*. It can be described as a conditional probability $R(\omega|\omega')$ that a scattering event with an energy transfer of ω' is registered in the channel ω. Accordingly, a true, 'theoretical' spectrum $S^{\mathrm{th}}(\omega')$ gives rise to an observed, 'experimental' spectrum

$$S^{\mathrm{ex}}(\omega) = \int \mathrm{d}\omega'\, R(\omega|\omega') S^{\mathrm{th}}(\omega'). \tag{29}$$

In QENS, it is a good approximation that R depends only on the energy difference, $R(\omega|\omega') = R(\omega - \omega')$. Under this assumption, (29) is a convolution integral,

$$S^{\mathrm{ex}} = R \otimes S^{\mathrm{th}} \tag{30}$$

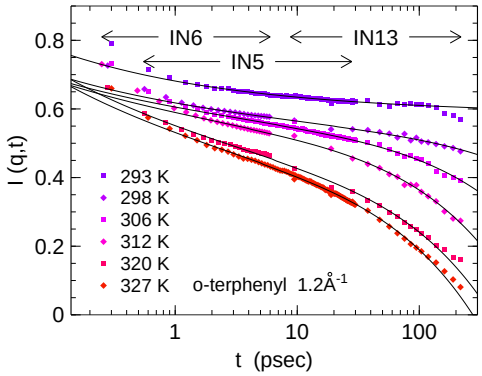

Fig. 3: *Intermediate scattering function of the glass-forming liquid ortho-terphenyl, measured on three different spectrometers of the ILL, and combined after Fourier deconvolution. Solid lines are fits with a mode-coupling scaling function. Redrawn from [5].*

for short, and R can be experimentally determined by measuring the spectrum of a material that is known to be a purely elastic scatterer, since $R \otimes \delta = R$.[4]

The resolution functions of time-of-flight and backscattering spectrometers are in a first approximation Gaussian. Typical scattering functions are qualitatively different in shape. When scaled for equal maximum and equal width at half maximum, a Lorentzian (and *a fortiori* a Kohlrausch-Williams-Watts function) has much broader wings than a Gaussian. In consequence, the onset of quasielastic scattering is regularly detected as additional scattering deep in the wings of the resolution function before any broadening is observed in the width at half maximum (Fig. 2). For this reason, in high-resolution neutron scattering the signal-to-noise ratio is a more important figure of merit than the nominal resolution width.

In principle, resolution effects can be removed from experimental data by Fourier deconvolution:

$$I^{\mathrm{th}}(t) = \frac{I^{\mathrm{ex}}(t)}{\tilde{R}(t)}. \tag{31}$$

The number of independent t points is limited by the Nyquist sampling theorem. For most of these t, (31) results in the division of two small, noisy numbers. Therefore one must introduce a cut-off time, restricting I^{th} to a relatively small number of short-time data points.

so that one has to restrict the computation to a relatively small number of short-time data points. This loss of information is normally not acceptable; instead of deconvoluting experimental data, it is preferable to fit the measured data S^{ex} with a theoretical function S^{th} that has been numerically convolved with the measured resolution R (or a smoothened model thereof). However, explicit Fourier deconvolution is attractive for combining spectral measurements from different spectrometers (Fig. 3) or for comparing neutron scattering with molecular dynamics simulations.

[4] Some phonon scattering can be tolerated in the resolution measurement, since it occurs mostly outside the energy window relevant for QENS. In practice, the resolution measurement is usually done either on vanadium (which is a perfectly incoherent scatterer so that the same measurement can also be used for detector calibration) or on the sample at low temperature (which has the advantage of being as close as possible to the conditions of the production measurements).

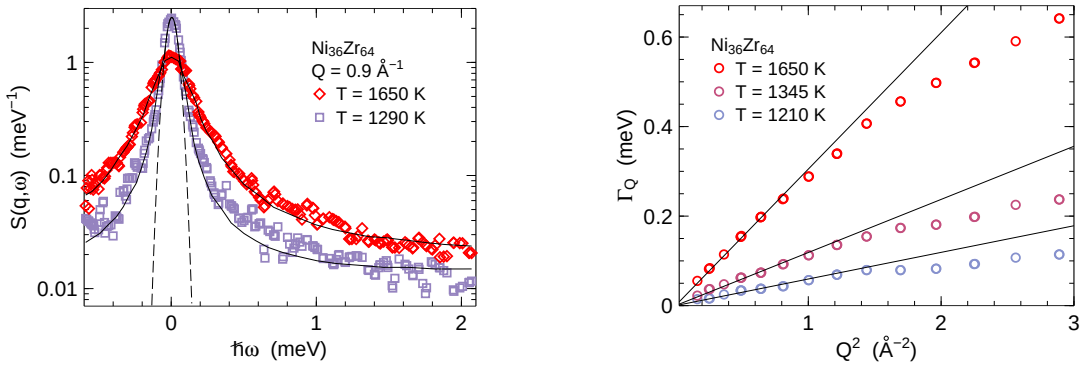

Fig. 4: *Atomic dynamics of liquid Zr-Ni, investigated with the time-of-flight spectrometer TOFTOF at FRM II, redrawn from [6]. (a) Selected spectra with Lorentzian fits (34). The dashed Gaussian with a FWHM of 95 μeV is an idealized representation of the instrumental resolution. (b) Linewidths Γ_Q, from Lorentzian fits to the measured spectra. For small Q, the scattering is dominated by incoherent contributions from Ni. Therefore, the initial slope of Γ_Q vs. Q^2 yields the self-diffusion coefficient of Ni.*

3 Application Examples

3.1 Diffusion

Diffusion has been discussed in much detail in lecture B3. To derive the incoherent scattering function for a diffusing particle, we equate the space-time probability distribution function $P(\mathbf{r}, t)$ introduced in section 2.2 of B3 with the classical approximation to the self-correlation function introduced in Eq. (9) of the present lecture. We can then immediately copy the solution of the standard diffusion equation,

$$G_{\mathrm{s}}^{\mathrm{cl}}(\mathbf{r}, t) = \frac{1}{(4\pi D t)^{3/2}} \mathrm{e}^{-r^2/4Dt}. \tag{32}$$

By Fourier transform, we find the intermediate scattering function

$$I(Q, t) = \exp(-DQ^2 t) = \tilde{\mathcal{L}}(t; DQ^2), \tag{33}$$

and by looking up (26) we obtain the scattering function

$$S(Q, \omega) = \mathcal{L}(\omega; DQ^2). \tag{34}$$

On a time-of-flight spectrometer, with experimental scales of the order $Q \sim \text{Å}^{-1}$ and $\hbar\omega \sim 0.1 \ldots 10$ meV, one can resolve diffusion coefficients D of the order $10^{-10} \ldots 10^{-8}$ m^2/s.

The straightforward determination of D from Lorentzian fits (34) works best in simple atomic systems. Recent examples are provided by metallic melts, which can be studied under very clean experimental conditions using electromagnetic levitation (Fig. 4). Results improve significantly upon macroscopic laboratory measurements that suffer from convective contributions.

In molecular liquids the applicability of (34) is not ascertained a priori because the atomic motion seen by neutron scattering is a superposition of molecular translation, molecular rotation, and innermolecular vibrations and rearrangements. This has been demonstrated very clearly in a systematic study of alkanes $\mathrm{C}_n\mathrm{H}_{2n+2}$ (Fig.5).

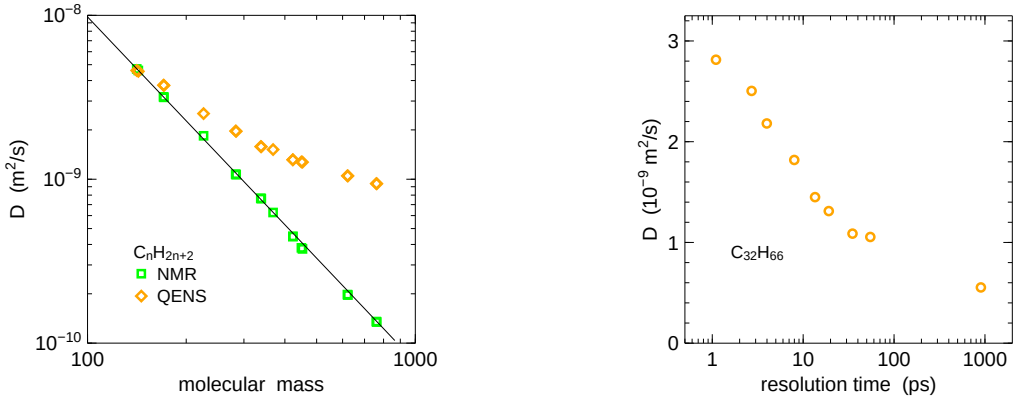

Fig. 5: *Hydrogen dynamics in n-alkanes. (a) Diffusion coefficient D, determined by pulsed-field gradient NMR and by neutron scattering using TOFTOF at FRM II. The Data points agree only for the shortest molecule ($n = 8$). In longer chains, QENS deviates from NMR because it measures not only center-of-mass molecular translation, but also rotation and innermolecular motion. Redrawn from [7]. (b) In an exemplary series of TOFTOF measurements with different instrumental resolutions (expressed through a resolution time), oversimplified fits have been shown to result in a resolution dependence of the apparent diffusion coefficients. Redrawn from [8].*

3.2 Jumps between two positions

In the simplest jump model, we consider jumps of a proton between two positions $\boldsymbol{r}_1$ and $\boldsymbol{r}_2$. This two-site jump model has only few applications, but it allows us to introduce concepts that come to fruition in the study of molecular rotation.

The probability $p(\boldsymbol{r}, t)$ of finding the proton at time t at site $\boldsymbol{r}$ obeys the rate equation

$$\frac{\mathrm{d}}{\mathrm{d}t}\begin{pmatrix} p(\boldsymbol{r}_1,t) \\ p(\boldsymbol{r}_2,t) \end{pmatrix} = -\begin{pmatrix} \lambda_1 & -\lambda_2 \\ -\lambda_1 & \lambda_2 \end{pmatrix}\begin{pmatrix} p(\boldsymbol{r}_1,t) \\ p(\boldsymbol{r}_2,t) \end{pmatrix} \tag{35}$$

with transition rates λ_n. The matrix has the eigenvalues 0 and $\Gamma := \lambda_1 + \lambda_2$, so that the rate equation is solved by $p(\boldsymbol{r}_n, t) = a_n + b_n \exp(-\Gamma t)$. In the long-time limit $t \to \infty$, the occupation ratio must be $p_1/p_2 = \lambda_2/\lambda_1$ to satisfy $\mathrm{d}p/\mathrm{d}t = 0$. Combined with the normalization condition $\sum_n p(\boldsymbol{r}_n, t) = 1$, we find

$$a_1 = p(\boldsymbol{r}_1, \infty) = \frac{\lambda_2}{\Gamma}, \quad a_2 = p(\boldsymbol{r}_2, \infty) = \frac{\lambda_1}{\Gamma}. \tag{36}$$

Imposing the initial condition $p(\boldsymbol{r}_1, 0) = 1$, we compute the conditional probabilities

$$\begin{aligned} p(\boldsymbol{r}_1, t|\boldsymbol{r}_1, 0) &= a_1 + a_2 \exp(-\Gamma t), \\ p(\boldsymbol{r}_2, t|\boldsymbol{r}_1, 0) &= a_2 \left(1 - \exp(-\Gamma t)\right), \end{aligned} \tag{37}$$

and similarly for $p(\boldsymbol{r}_2, 0) = 1$. Using the equilibrium occupation probabilities (36), and introducing the jump vector $\boldsymbol{d} := \boldsymbol{r}_2 - \boldsymbol{r}_1$, we obtain the intermediate self correlation function

$$\begin{aligned} I(\boldsymbol{Q}, t) &= \langle \mathrm{e}^{i\boldsymbol{Q}\boldsymbol{r}(t)} \mathrm{e}^{-i\boldsymbol{Q}\boldsymbol{r}(0)} \rangle \\ &= p(\boldsymbol{r}_1, \infty)\left[p(\boldsymbol{r}_1, t|\boldsymbol{r}_1, 0) + p(\boldsymbol{r}_2, t|\boldsymbol{r}_1, 0)\mathrm{e}^{i\boldsymbol{Q}\boldsymbol{d}}\right] + \\ &\quad p(\boldsymbol{r}_2, \infty)\left[p(\boldsymbol{r}_2, t|\boldsymbol{r}_1, 0) + p(\boldsymbol{r}_1, t|\boldsymbol{r}_1, 0)\mathrm{e}^{-i\boldsymbol{Q}\boldsymbol{d}}\right]. \end{aligned} \tag{38}$$

Regrouping terms, abbreviating

$$\begin{aligned} A_0(\boldsymbol{Q}) &:= a_1^2 + a_2^2 + 2a_1a_2 \cos \boldsymbol{Qd}, \\ A_1(\boldsymbol{Q}) &:= 2a_1a_2(1 - \cos \boldsymbol{Qd}), \end{aligned} \tag{39}$$

and evaluating the Fourier transform of $\exp(-\Gamma t)$, we get the incoherent scattering function

$$S(\boldsymbol{Q}, \omega) = A_0(\boldsymbol{Q})\delta(\omega) + A_1(\boldsymbol{Q})\mathcal{L}(\omega; \Gamma), \tag{40}$$

which consists of an elastic line and a quasielastic component, the latter having standard Lorentzian shape (26). As discussed above, the presence of an elastic line is characteristic for *localized motion*: Since the jumping proton is confined to a finite region in space, its self correlation function never decays to zero.

For measurements performed on powder samples, we average over the orientations of $\boldsymbol{d}$,

$$\overline{\cos \boldsymbol{Qd}} = \frac{1}{4\pi} \int_0^\pi \mathrm{d}\vartheta \, 2\pi \sin\vartheta \, \cos(Qd \cos\vartheta) = \frac{\sin Qd}{Qd} = j_0(Qd), \tag{41}$$

where the last equation introduces a customary abbreviation, the spherical Bessel function j_0. In the simplest case, for jumps between two equivalent positions, we have $\lambda_1 = \lambda_2$ and $a_1 = a_2 = 1/2$, so that the powder-averaged amplitudes take the form

$$\begin{aligned} A_0(Q) &= (1 + j_0(Qd))/2, \\ A_1(Q) &= (1 - j_0(Qd))/2. \end{aligned} \tag{42}$$

3.3 Rotational jump diffusion

To discuss the rotation of molecules or molecular side groups in solids we choose a simple and practically important example, a methyl group R–CH_3. We consider the group as stiff (CH bond length $d = 1.097 \pm 0.004$ Å, HCH angle $\theta = 106.5 \pm 1.5°$). The only degree of freedom is the rotation around the bond that connects the methyl group to the remainder R of the molecule. This R–C bond coincides with the symmetry axis of the CH_3 group. The corresponding moment of inertia is

$$I = \sum m d_\perp^2 = 2md^2(1 - \cos\theta). \tag{43}$$

The rotational motion can be described by a wave function ψ that depends on one single coordinate, the rotation angle ϕ. The Schrödinger equation is

$$\left\{ B\frac{\partial^2}{\partial\phi^2} - V(\phi) + E \right\} \psi(\phi) = 0 \tag{44}$$

with the *rotational constant*

$$B := \frac{\hbar^2}{2I} = 670 \ \mu\mathrm{eV}. \tag{45}$$

For free rotation ($V = 0$), solutions that possess the requested periodicity are sine and cosine functions of argument $J\phi$, with integer J. Accordingly, the energy levels are $E = BJ^2$.

In condensed matter, however, the potential V caused by the local environment cannot be neglected. Due to the symmetry of the CH_3 group, the Fourier expansion of $V(\phi)$ contains

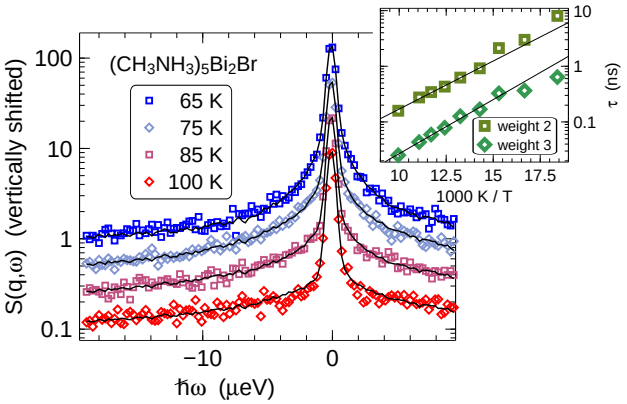

Fig. 6: *Backscattering spectra of $(CH_3NH_3)_5Bi_2Br$, measured on SPHERES [9]. The five methylammonium cations fall into two different categories: at room temperature, two of them are ordered, three are disordered [10]. Therefore, we fitted the spectra with two Lorentzians with an amplitude ratio of 2:3. The resulting relaxation times have an Arrhenius temperature dependence, shown in the inset.*

only sine and cosine functions with argument $3m\phi$, with integer m. In most applications, it is sufficient to retain only one term,

$$V(\phi) \doteq V_3 \cos(3\phi). \tag{46}$$

The strength of the potential can then be expressed by the dimensionless number V_3/B. In the following we specialize to the case of a *strong potential*, $V_3/B \gg 10$, which is by far the most frequent one.

In a strong potential of form (46), the CH_3 group has three preferential orientations, separated by potential walls. The motion of the CH_3 group consists mainly of small excursions from the preferred orientations, called *librations*. Quantum-mechanically, they are zero-point oscillations in an approximately harmonic potential.

Orientational motion can be approximated as thermally activated *jump diffusion* between equivalent equilibrium positions. For instance, to compute incoherent scattering from a rotating methyl (CH_3) group, it can be sufficient to consider 120° jumps between three equivalent rest positions on a circle of radius r.

This requires only a little extension of the two-site jump model introduced above. The transition matrix in the rate equation takes the form

$$\begin{pmatrix} 2\lambda & -\lambda & -\lambda \\ -\lambda & 2\lambda & -\lambda \\ -\lambda & -\lambda & 2\lambda \end{pmatrix}, \tag{47}$$

which has the eigenvalues 0, 3λ, 3λ. Thanks to the degeneracy of the nonzero eigenvalue, the scattering law retains the simple form (40), with $\Gamma = 3\lambda$, and with amplitudes

$$\begin{aligned} A_0(Q) &= (1 + 2j_0(Qr\sqrt{3}))/3, \\ A_1(Q) &= (2 - 2j_0(Qd\sqrt{3}))/3. \end{aligned} \tag{48}$$

This model has proven successful in a huge number of experiments; Fig. 6 shows an arbitrarily chosen recent example.

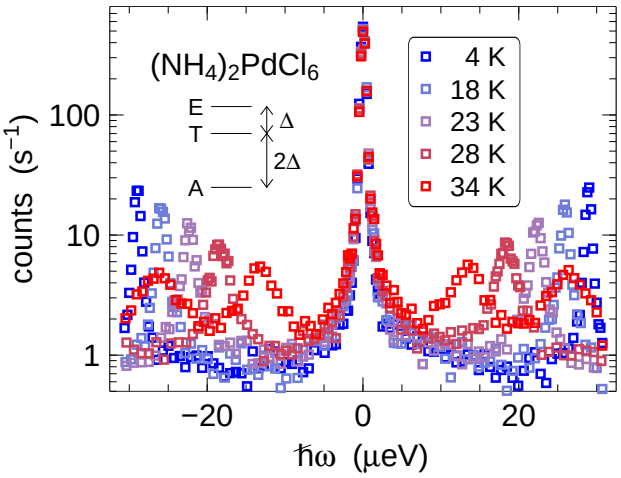

Fig. 7: *Backscattering spectra of the perovskite $(NH_4)_2PdCl_6$, measured on SPHERES [12]. The inelastic lines are due to rotational tunneling of the NH_4^+ group. The energy-level scheme holds for tetrahedral symmetry at the NH_4^+ sites if the probability of 180° jumps is negligible compared to 120° jumps [13]. Only the E↔T transition is observed, except at 34 K where also the A↔T transition fits into the experimental energy range.*

However, Eq. (40) must be modified if the rotational potential has a C_2 symmetry. Then there are six equivalent equilibrium positions, connected by 60° jumps, so that the transition matrix is of rank 6. After some computation it is found to have three different non-zero eigenvalues Γ_μ. In such a situation, the inelastic part of scattering law no longer factorises into a Q dependent and a ω dependent function. Instead, one has a sum of Lorentzians of different widths:

$$S(\boldsymbol{Q},\omega) = A_0(\boldsymbol{Q})\delta(\omega) + \sum_\mu A_\mu(\boldsymbol{Q})\mathcal{L}(\omega;\Gamma_\mu). \tag{49}$$

This equation holds quite generally for systems described by a rate equation of the form (35) with an arbitrary, symmetric transition matrix. In particular, it holds for rotational jump diffusion of molecules that have more than one axis of rotation [11].

3.4 Rotational tunneling

At low temperatures, almost exclusively the vibrational ground state is occupied. Yet reorientational motion beyond librations is possible by means of quantum mechanical tunneling: The wave functions of the three localised *pocket states* ψ_m ($m = 1,2,3$) have nonzero overlap. Therefore, the eigenstates are a linear combination of pocket states.[5] Periodicity and threefold symmetry allow three such combinations: a plain additive one

$$\psi_1 + \psi_2 + \psi_3, \tag{50}$$

and two superpositions with phase rotations

$$\psi_1 + \mathrm{e}^{\pm i2\pi/3}\psi_2 + \mathrm{e}^{\pm i4\pi/3}\psi_3. \tag{51}$$

[5]This is an extremely simplified outline of the theory. In a serious treatment, to get all symmetry requirements right, one must also take into account the nuclear spins of the H atoms [14].

In the language of group theory, state (50) has symmetry A, the degenerate states (51) are labelled E^a, E^b. It is found that A is the ground state. The *tunneling splitting* $\hbar\Omega_\mathrm{t}$ between the states A and E is determined by the overlap integral $\langle\psi_m|V|\psi_n\rangle$ ($m \neq n$), which depends exponentially on the height of the potential wall. Experiments that detect tunneling transitions provide therefore a very sensitive probe of the rotational potential; conversely, if the potential is not accurately known, it is almost impossible to predict whether a tunneling transition will show up in a given experimental energy range.

In neutron scattering, a tunneling transition appears as a pair of inelastic peaks at $\pm\hbar\Omega_\mathrm{t}$. The spectral shape of these peaks is well described by Lorentzians $\mathcal{L}(\omega \pm \Omega_\mathrm{t}; \Gamma)$. With rising temperatures, the occupancy of excited vibrational levels increase. This facilitates transitions between A and E sublevels and results in a decrease of $\hbar\Omega_\mathrm{t}$ and an increase of the line width Γ.

Upon further temperature increase, thermal motion of neighbouring molecules causes so strong potential fluctuations that the picture of quantum tunneling is no longer applicable. Instead, the motion between different pocket states must be described as *stochastic jump diffusion*, as exposed above.

For systems with more than one rotational axis, group theory is used to identify eigenstate symmetries. For instance for tetrahedral NH_4^+ ions in tetrahedral cages, three energy levels are found, with a transition energy ratio of $\Omega_\mathrm{TA} = 2\Omega_\mathrm{ET}$ (Fig. 7).

References

[1] N. W. Mermin, J. Math. Phys. **7**, 1038 (1966).

[2] W. Doster, S. Cusack and W. Petry, Nature **337**, 754 (1989).

[3] W. Doster, Eur. Biophys. J. **37**, 591 (2008).

[4] W. Doster, S. Busch, A. M. Gaspar, M. S. Appavou, J. Wuttke and H. Scheer, Phys. Rev. Lett. **104**, 098101 (2010).

[5] J. Wuttke, M. Kiebel, E. Bartsch, F. Fujara, W. Petry and H. Sillescu, Z. Phys. B **91**, 357 (1993).

[6] D. Holland-Moritz, S. Stüber, H. Hartmann, T. Unruh, T. Hansen and A. Meyer, Phys. Rev. B **79**, 064204 (2009).

[7] C. Smuda, S. Busch, G. Gemmecker and T. Unruh, J. Chem. Phys. **129**, 014513 (2008).

[8] T. Unruh, C. Smuda, S. Busch, J. Neuhaus and W. Petry, J. Chem. Phys. **129**, 121106 (2008).

[9] A. Piecha, J. Wuttke, R. Jakubas and G. Bator, JCNS experimental report 3961 (2010).

[10] J. Matuszewski, R. Jakubas, L. Sobczyk and T. Głowiak, Acta Cryst. C **46**, 1385 (1990).

[11] M. Bée, *Quasielastic Neutron Scattering*, Adam Hilger: Bristol (1988).

[12] J. Wuttke, JCNS experimental report 2888 (2010).

[13] A. Hüller, Phys. Rev. B **16**, 1844 (1977).

[14] W. Press, *Single-particle rotation in molecular crystals* (Springer tracts in modern physics 92), Springer: Berlin (1981).